Scientia Iranica A (2011) 18 (4), 895–905

Sharif University of Technology

Scientia Iranica

Transactions A: Civil Engineering

www.sciencedirect.com

An updated study on near-fault ground motions of the 1978 Tabas, Iran, earthquake ($M_w = 7.4$)

S. Yaghmaei-Sabegh [a,*], **H.H. Tsang** [b]

[a] *Department of Civil Engineering, University of Tabriz, Tabriz, P.O. Box 51666-16471, Iran*

[b] *Department of Civil Engineering, University of Hong Kong, Hong Kong*

Received 12 December 2010; revised 21 May 2011; accepted 5 July 2011

KEYWORDS

Near-fault;
Ground motion;
Directivity;
Dynamic corner frequency;
Tabas earthquake;
Iran.

Abstract This paper presents an updated study and numerical modelling of the Tabas, eastern Iran earthquake ($M_w = 7.4$), which occurred on September 16, 1978, using new techniques recently proposed by various researchers. Firstly, the near-fault ground motions recorded at a station very close to the fault were examined based on the characteristics of the velocity pulses and the frequency content of the motions. Evidence of directivity effects in recorded, near-fault ground motion, has been investigated using various methods. In the second part of this paper, stochastic simulations of near-fault, strong ground motion, using finite-fault modelling, based on a dynamic corner frequency recently proposed by Motazedian and Atkinson [Motazedian, D. and Atkinson, G. "Stochastic finite-fault modelling based on a dynamic corner frequency", *Bull. Seismol. Soc. Amer.*, 95(2), pp. 995–1010 (2005)], have been presented. In order to model the impulsive behaviour of near-fault ground motion, the finite-fault model was combined with the mathematical expression of Mavroeidis and Papageorgiou [Mavroeidis, G.P. and Papageorgiou, A.S. "A mathematical representation of near-fault ground motions", *Bull. Seismol. Soc. Amer.*, 3, pp. 1099–1131 (2003)] for modelling pulse characteristics. A new set of modelling parameters has been recommended and good agreement has been found between the recorded and simulated response spectra. The velocity pulses observed in near-fault ground motion records could also be mimicked.

1. Introduction

On September 16, 1978, a destructive earthquake with moment magnitude of 7.4 occurred in the East-Central region of Iran, causing extensive damage to the city of Tabas and its surrounding area, with a fatality rate of more than 80% [1]; total death toll has been estimated as more than 15,000 [2,3]. The earthquake occurred on a thrust fault that had not been recognized in eastern Iran, and which extended over 80 km of distributed and discontinuous surface ruptures above a series of low anticlinal hills to the west of a major range-front [4].

Characteristics of ground motion close to an earthquake source can be considerably different from those of far-field motion. Accurate characterization and modelling of this motion is an imperative concern, in particular for the design of important engineering structures located near active faults. The motivation to study near-fault ground motion characteristics was induced following the 1966 earthquake in Parkfield, California, USA, and the 1971 earthquake in San Fernando, California, USA [5,6]. Over the past two decades, severe damage, as well as the failure of engineered structures, was observed within the near-fault regions in several major earthquake events, including the ones in Northridge, California, USA (1994), Kobe, Japan (1995), Chi-Chi, Taiwan (1999), and Bam, Iran (2003). These events revealed the vulnerability of existing structures against pulse-type ground motion [7–11]. Recent research has also shown the important effects of near-fault ground motion on the dynamic response of structures [12,13]. Meanwhile, accurate modelling of structural responses subjected to near-fault pulse-type loading requires a more thorough understanding of the pulse characteristics of the near-fault motion. Hence, a critical analysis of precious near-field records from this event has been conducted and the nearest strong ground motion data recorded at the Tabas station (TAB) with observed impulsive behaviour, have been selected for this

* Corresponding author.
E-mail address: s_yaghmaei@tabrizu.ac.ir (S. Yaghmaei-Sabegh).

1026-3098 © 2011 Sharif University of Technology. Production and hosting by Elsevier B.V. All rights reserved. Peer review under responsibility of Sharif University of Technology.

doi:10.1016/j.scient.2011.07.018

Production and hosting by Elsevier

study. It is noted that near-fault ground motion data have rarely been recorded in Iran. Hence, the results and insights obtained in this study could serve as a good resource for understanding near-fault ground motion characteristics in Iran, as well as in other regions with inadequate near-fault ground motion data.

2. Analytical modelling of impulsive behaviour

Severe damage is commonly observed in the vicinity of a fault rupture, referred to as "near-fault". Near-fault ground motion is distinguished from ordinary ground motion by its strong coherent long-period pulses and permanent ground displacements. Long-period pulses are generated in the horizontal direction perpendicular to the strike of the fault, due to rupture directivity effects [14,15]. Consequently, the dynamic response of structures induced by such motion deserves special consideration. There has been an increasing interest in the engineering community to investigate the effects of near-fault ground motion on the elastic and inelastic behaviour of engineered structures [16–19]. Previous studies [20–22] show that long-period pulses in near-fault ground motion are predominantly more critical to structures rather than the high shaking level. This type of ground motion may generate large energy demands that need to be dissipated by structures in a few large displacement excursions.

In the past decade, noteworthy progress has been made in improving our understanding of earthquake ground shaking in near-field areas, and much effort has been extended by seismologists to develop a reliable approach for modelling near-fault motion, in particular the impulsive nature of the motion. Currently, various simulation techniques exist and the analytical approach proposed by Mavroeidis and Papageorgiou [23] has been adopted in this study to model the near-fault motion of the 1978 Tabas earthquake. In this approach, four key parameters are used to define the waveform characteristics of the near-fault velocity pulses, namely, pulse duration, pulse amplitude, and number and phase of half cycles. The mathematical formulation of this effective, yet simple, model for simulating ground motion time histories with long-period impulses, acc(t), is shown in Eq. (1):

$$\begin{aligned}\mathrm{acc}(t) = &-\frac{A_{mp}\pi f_p}{\gamma} \\ &\times \left[\begin{array}{c} \sin\left(\dfrac{2\pi f_p}{\gamma}(t-t_0)\right)\cos[2\pi f_p(t-t_0)+\nu] \\ +\gamma\sin[2\pi f_p(t-t_0)+\nu]\left[1+\cos\left(\dfrac{2\pi f_p}{\gamma}(t-t_0)\right)\right]\end{array}\right], \\ &\text{for } t_0-\frac{\gamma}{2f_p}\le t\le t_0+\frac{\gamma}{2f_p} \text{ with } \gamma>1, \end{aligned} \quad (1)$$

where A_{mp}, f_p, ν, γ and t_0 are respectively, pulse amplitude, prevailing frequency, phase angle, oscillatory characteristic and time shift for mimicking the envelope of the long-period pulse. It is noted that the basic feature of Eq. (1) has been developed based on the Gabor wavelet [24], which is also defined by similar parameters to those shown in Eq. (2):

$$f(t) = A_{mp}\mathrm{e}^{-(2\pi f_p/\gamma)^2 t^2}\cos(2\pi f_p t+\nu). \quad (2)$$

Mavroedis and Papageorgiou [23] have, however, replaced the Gaussian envelope function of the Gabor wavelet by a symmetric bell-shaped function that leads to the functional form of Eq. (1). Details of this method can be found in [23].

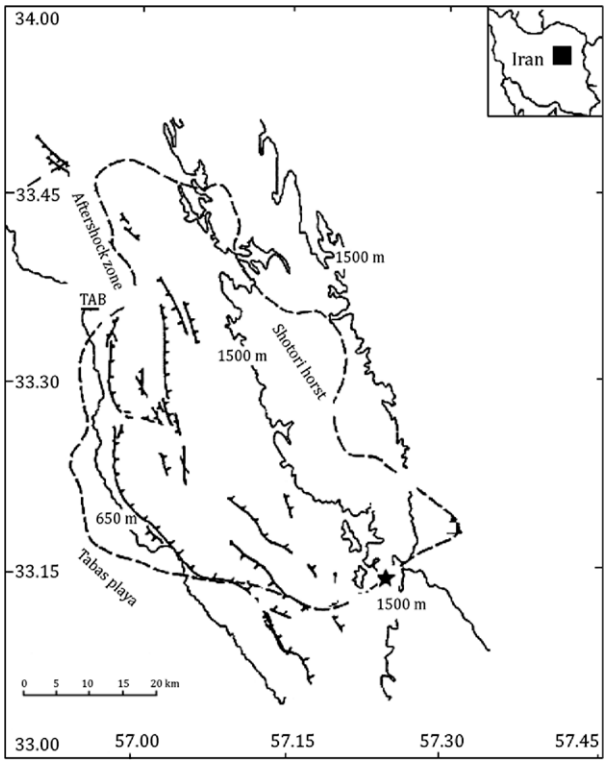

Figure 1: Map showing the epicenter of Tabas earthquake annotated by a solid star symbol [28], and the location of Tabas station (abbreviated as TAB) annotated by a solid triangle.

An important characteristic of this analytical model is the objective definition of the pulse duration (T_p), which is based on the reciprocal of the prevailing frequency of the signal (f_p):

$$T_p = \frac{1}{f_p}. \quad (3)$$

This analytical approach has effectively simulated the observed impulsive behaviour found in the near-fault records of the M 7.2, 1992 Landers earthquake in California, USA [25] and the M 6.5, 2003 Bam earthquake in Iran [26].

3. Analysis of directivity effects

Data employed in this study were collected from the strong ground motion database of the Pacific Earthquake Engineering Research (PEER) Center (www.peer.berkeley.edu). Ground motions were recorded by 11 accelerograph stations, with epicentral distances ranging from 3 to 350 km, and corresponding peak accelerations ranging from 0.01 to 0.95 g. According to the study conducted by Yaghmaei-Sabegh [27], among the 11 stations, near-fault ground motion pulses could only be observed in the data recorded at the station nearest to the epicentre, namely, Tabas station (TAB). Hence, the ground motion recorded at the Tabas station has been used in the analysis in this study. Figure 1 shows the epicentre (33.6° N 56.9° E) of the Tabas earthquake, as annotated by a solid star symbol, and the location of the Tabas station (abbreviated as TAB), as annotated by a solid triangle [28].

Evidence of near-fault ground motion characteristics has been observed in both field observations and recorded strong ground motion data. The large-amplitude displacement pulses have led to an increase in damage in the vicinity of the source

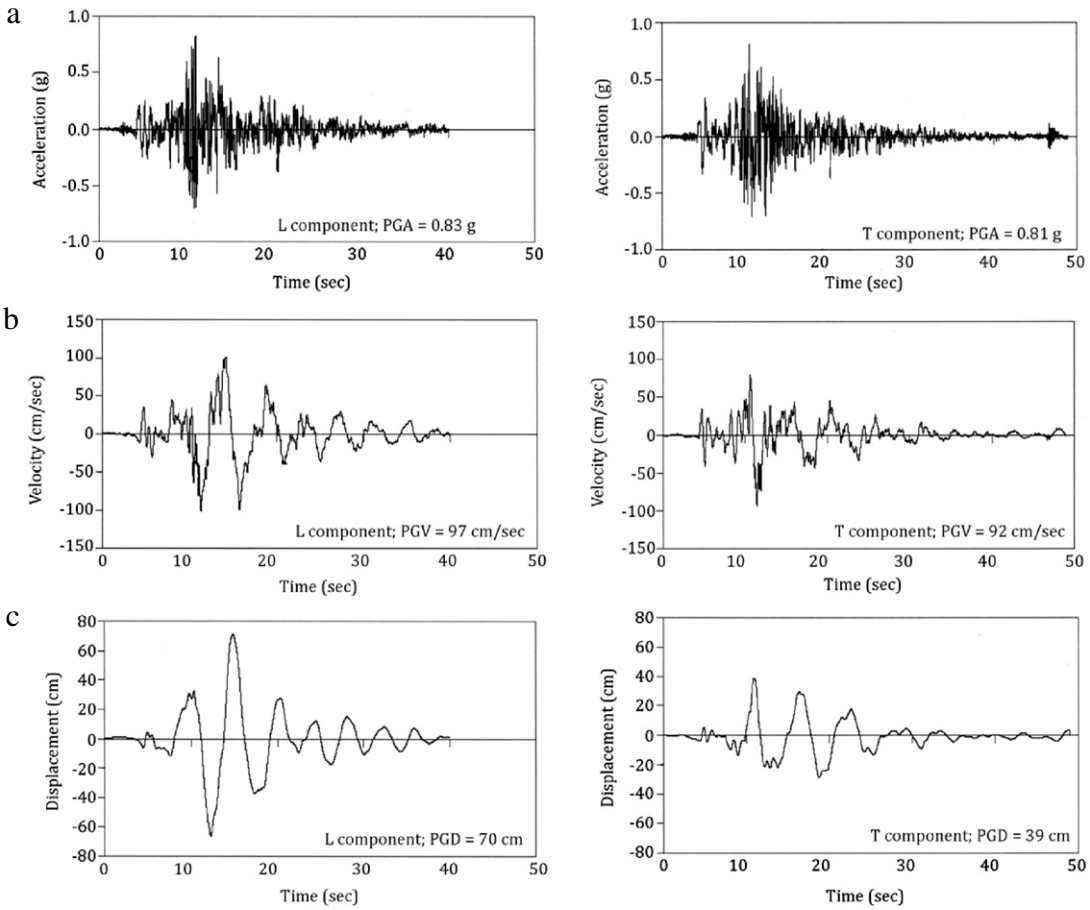

Figure 2: (a) Acceleration, (b) velocity, and (c) displacement time histories of M 7.4 1978 Tabas earthquake recorded at Tabas station (L, T component). *Source:* Strong ground motion database of Pacific Earthquake Engineering Research (PEER) Center (www.peer.berkeley.edu).

region. This evidence has been validated by various methods and summarized in this section. The pulse, with duration of 5.1 s, recorded during this major earthquake in Iran, is one of the distinctive pulses from among other near source motion recorded in other parts of the world.

The horizontal components of the acceleration, velocity and displacement ground motion time histories recorded by the Tabas station are shown in Figure 2. An important feature of this record is the location of the pulse. The pulse typically occurs at the beginning of the time history, while the pulse in this record occurs closer to the middle. It is also observed that the acceleration ground motion time history is packed with high frequency spikes, without an obvious acceleration pulse. In this section, three different indicators of directivity effects have been used for investigating near-fault motion recorded during the Tabas earthquake.

3.1. Duration of velocity pulse

It is well-known that a key feature of forward-rupture directivity is the presence of large velocity pulses in the fault-normal component of ground motion. In order to search for evidence of rupture directivity effects in strong ground motion, the data were first rotated to the fault-normal and fault-parallel directions, as shown in Figure 3. The rotation was performed by a simple vector rotation method, as introduced by Somerville et al. [14].

The first indicator of directivity effects is the pulse period (or pulse duration). This parameter is more commonly known in the field of structural engineering as the ratio of pulse period to fundamental period of the structure (T_p/T), which can significantly affect structural responses [9]. There is no consistent definition for a pulse period; however, this parameter is extensively used in literature (for examples [15,29,30]). In this study, an objective definition of the pulse period proposed by Mavroeidis and Papageorgiou has been adopted [23], which is compatible with the physical meaning, as the inverse of the prevailing frequency (refer to Eq. (3)). In [23], 165 near-field ground motion time histories recorded from earthquakes of different fault rupture mechanisms and covering a wide range of magnitude ($5.6 < M_w < 8.1$) have been used to derive a relationship between the pulse period and moment magnitude (M_w) of an earthquake, as follows:

$$\log_{10}(T_p) = -2.2 + 0.4M_w. \quad (4)$$

It is noted that the analytical approach of Mavroeidis and Papageorgiou [23] for modelling pulse motion has also been adopted in the second part of this study.

More recently, a new relationship has been developed by Baker [31] to determine the pulse period for pulse-like motion, based on a continuous wavelet analysis, as follows:

$$\ln(T_p) = -5.78 + 1.02M_w. \quad (5)$$

The predicted period values for the dominant velocity pulse in the fault-normal component of the ground motion of this

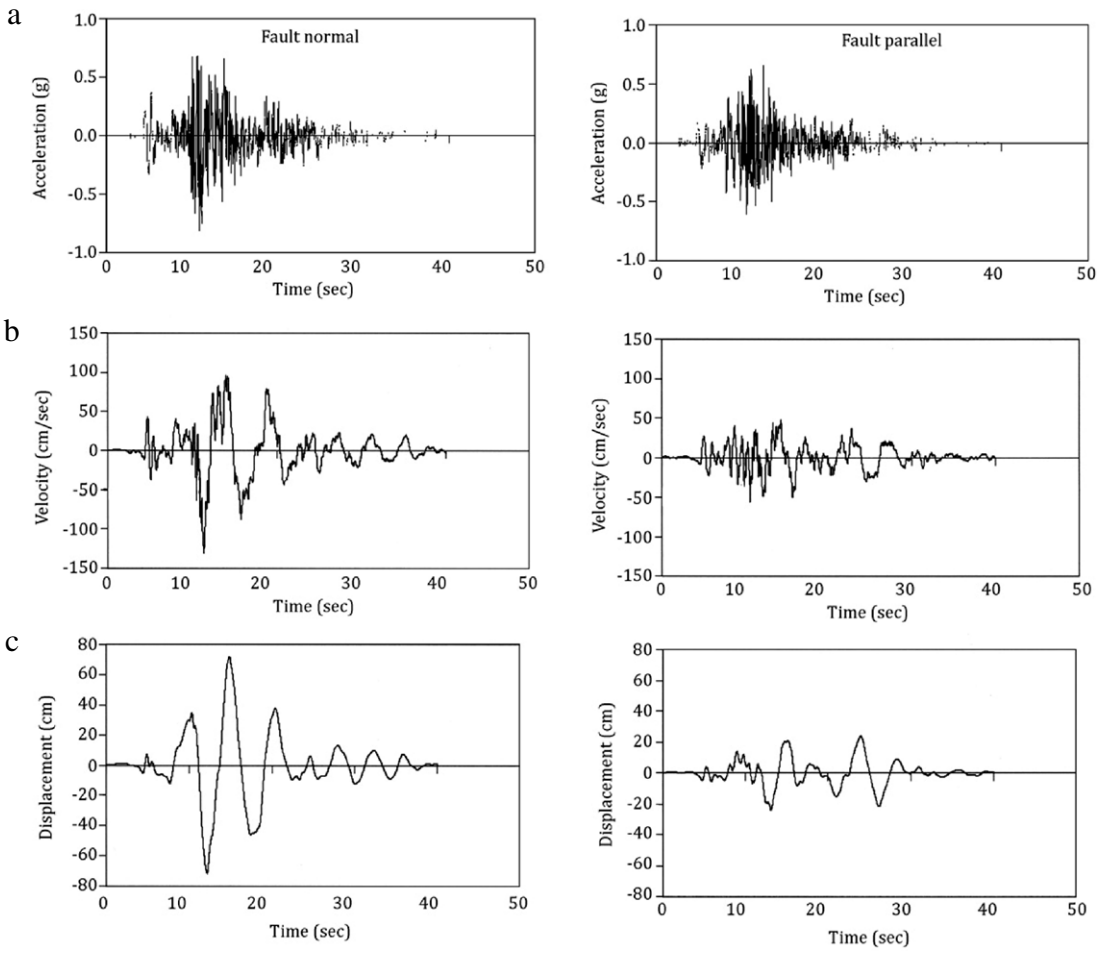

Figure 3: Fault-normal and fault-parallel components of the (a) acceleration, (b) velocity, and (c) displacement time histories recorded at Tabas station, rotated using simple vector rotation method.

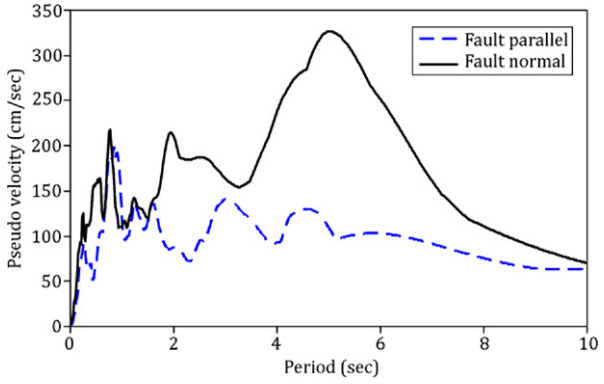

Figure 4: 5% damped pseudo-velocity response spectra of the fault-normal and fault-parallel components of ground motion recorded at Tabas station.

M_w 7.4 Tabas earthquake are 5.75 s and 5.85 s, respectively, according to Eqs. (4) and (5). It is noteworthy that these two values obtained using two independent relationships, are consistent with each other. As shown in Figure 4, there is a dominant peak in the pseudo-velocity response spectrum of the fault-normal component at a period of 5.1 s, which is broadly supported by the predicted values based on Eqs. (4) and (5). The wavelet-based period is larger than the spectral velocity-based period, which is consistent with previous findings from other studies [15,31].

3.2. Peak ground velocity

On the other hand, the value of the peak ground velocity of the fault-normal component can be estimated by the empirical relation proposed by Bray and Rodriguez-Marek [15], which was developed using a database consisting exclusively of forward-directivity records measured on rock sites, as follows:

$$\ln(\mathrm{PGV}) = 4.46 + 0.34M_w - 0.58\ln(R^2 + 7^2) \pm 0.39, \qquad (6)$$

where R is the closest distance from the site to the rupture surface (Rrup) in km, PGV is peak ground velocity in cm/s, and the last term (± 0.39) is the standard deviation (in logarithmic scale) of the predictions, which could be translated to $\pm 48\%$ in linear scale.

The peak ground velocity value recorded at the Tabas station is 125 cm/s, which is less than 20% different from the value of 154 cm/s predicted by Eq. (6).

Bray and Rodriguez-Marek have also used the ratio between fault-parallel to fault-normal peak ground velocity values as an evidence of forward rupture directivity [15]. The ratio was found to have a median value of 0.65, with a standard deviation of 0.25. In this study, this ratio is calculated as 0.79, which is within one standard deviation from the proposal of Bray and Rodriguez-Marek [15].

Table 1: Summary of the examination of directivity effects in the near-fault ground motion recorded at Tabas station.

Items	Methods	Results
Duration of velocity pulse	Mavroeidis and Papageorgiou [23] $\log_{10}(T_p) = -2.2 + 0.4M_w$	5.75 s
	Baker [31] $\ln(T_p) = -5.78 + 1.02M_w$	5.85 s
	Data recorded at Tabas station	5.1 s
Peak ground velocity	Bray and Rodriguez-Marek [15] $\ln(\text{PGV}) = 4.46 + 0.34M_w - 0.58\ln(R^2 + 7^2) \pm 0.39$	154 cm/s
	Data recorded at Tabas station	125 cm/s
Spectral response ratio	Somerville et al. [14]	Graphical results referred to Figure 5

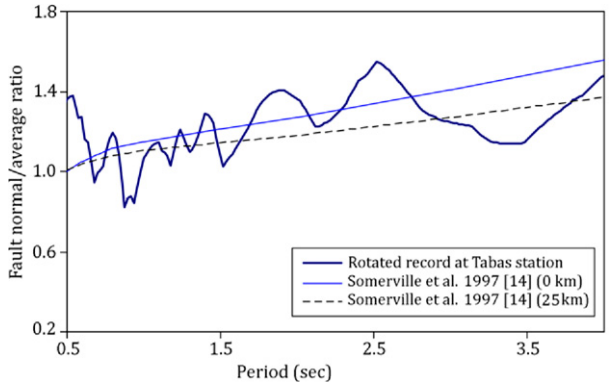

Figure 5: Ratio of the fault-normal to average horizontal response spectra of ground motions recorded at Tabas station.

3.3. Spectral response ratio

Forward rupture directivity can also be indicated by the ratio of the fault-normal horizontal response spectrum to the average horizontal response spectrum [14,32]. Such a ratio, calculated from the Tabas records, has been plotted in Figure 5, and superimposed with the proposals in [14]. It is shown that the ratio is comparable, with larger values at certain period ranges, to those estimated by Somerville et al. [14].

A summary of the analysis of directivity effects in near-fault ground motion recorded at the Tabas station, using various methods, has been tabulated in Table 1.

4. Stochastic simulation of seismological model

4.1. Point-source $\omega 2$ model

The stochastic method is widely used for simulating acceleration time histories of earthquake motion, and subsequently for developing a ground-motion prediction equation, which is the fundamental element for a seismic hazard assessment study [33–39]. Ground motion time histories are also required for engineering analyses of the responses of structures subject to earthquake shaking. Extensive literature is available on the subject of the stochastic simulation method [37,40]; hence only a brief review of the key features of the seismological model is provided herein. The original form of the Fourier amplitude spectrum of ground motion can simply be modelled by an $\omega 2$ model, where ω is the angular frequency [41–43].

The acceleration amplitude of the spectrum, $A(f)$, can be expressed as:

$$A(f) = CM_0(2\pi f)^2/[1 + (f/f_0)^2] \times \exp(-\pi f\kappa)\exp(-\pi fR/Q\beta)/R, \quad (7)$$

where f is frequency, R is hypocentral distance, M_0 is seismic moment in dyne cm, f_0 is corner frequency, and β is the shear wave velocity of the rock crust in km/s [43]. The constant $C = \Re_{\theta\varphi}FV/(4\pi\rho\beta^3)$ in which $\Re_{\theta\varphi}$ is the radiation pattern (average value of 0.55 for shear waves), F is free-surface amplification (2.0), V is the partition into two horizontal components (0.71) and ρ is the density of the rock crust [43]. High-frequency ground motion would be attenuated along the travelling path of the seismic waves, and the rate of attenuation can be characterized by $\exp(-\pi fR/Q\beta)$ in which the quality factor, $Q(f)$, is an inverse measure of the anelastic attenuation properties of the rock crust. For the attenuation properties at the near surface of the rock crust, another expression, $\exp(-\pi f\kappa)$, is used in which the decay parameter, "kappa (κ)", has been defined to represent the attenuation properties of rock crust at the near surface (in the order of 4 km depth) [44].

4.2. Finite-fault model

The simple point-source $\omega 2$ model has been extensively adopted, which has been proved to be a valid and reliable method for simulating earthquake ground motion time histories. However, it is recognised that the point-source model may be inadequate for modelling the near-source ground motion of large earthquakes [45]. To overcome this limitation, point-source modelling has been extended to finite-fault modelling, by dividing a large fault into N subfaults of which each subfault is considered a point source. This technique is developed, based on the original idea of Hartzell [46], to model large earthquakes by the summation of smaller ones with a proper time delay in the time domain. The time delay for a subsource is given by the time required for the rupture to reach the subsource (from hypocenter), plus the time for the radiated wave to propagate from the subsource to the site (receiver). This approach has been applied widely for the prediction of ground motion near the epicentres of large earthquakes [45,47–49].

4.3. Dynamic behaviour of finite-fault model

More recently, Motazedian and Atkinson [25] further developed the finite-fault modelling technique by introducing a new concept of "dynamic corner frequency" to achieve a more realistic modelling of the dynamic behaviour of the finite-fault. In this advanced approach, the Fourier spectrum of acceleration amplitude for the ijth subfault on the fault plane at a distance, R_{ij}, can be modelled as a point source by modifying Eq. (7) as follows:

$$A_{ij}(f) = CM_{0ij}H_{ij}(2\pi f)^2/[1 + (f/f_{0ij})^2] \times \exp(-\pi f\kappa)\exp(-\pi fR_{ij}/Q\beta)/R_{ij}, \quad (8)$$

Table 2: Information from stations whose recorded ground motion was used for determining quality (Q) factor.

Station name	Coordinates		Distance (km)
	Latitude (N)	Longitude (E)	
Tabas	33.6	55.92	3
Deyhook	33.3	57.52	18
Booshroyeh	33.88	57.43	40
Ferdows	34.03	58.81	115
Khezri	34.03	58.81	160
Bajestan	34.51	58.18	161
Sedeh	33.33	59.2	172
Birjand	32.86	59.2	175
Kashmar	35.5	58.45	250

Notes: Distance given in the table is the hypocentral distance (with focal depth of 9 km) except for Tabas station which is the shortest distance to the fault plane.

where M_{0ij} and R_{ij} are the seismic moment of the ijth subfault and the distance from the center of the subfault to the observation point, respectively. The dynamic corner frequency of the ijth subfault, $f_{0ij}(t)$, proposed by Motazedian and Atkinson is given by [25]:

$$f_{0ij}(t) = 4.9 \times 10^6 \beta (\Delta\sigma / M_{0ave})^{1/3} N_R(t)^{-1/3}, \quad (9)$$

where t is the time for the ijth subfault to be triggered; $N_R(t)$ is the cumulative number of ruptured subsources at time t; $M_{0ave} = M_0/N$ is the average seismic moment of subfaults; N is the total number of subfaults; and $\Delta\sigma$ is the stress drop in bars. The scaling factor, H_{ij}, for the ijth subfault in Eq. (8) is applied to conserve the energy of seismic waves at high frequencies, and is defined based on the summing up of all frequencies of the spectrum for the ijth subfault:

$$H_{ij} = \left[\frac{N \sum_f \left(\frac{f^2}{1+(f/f_0)^2} \right)^2}{\sum_f \left(\frac{f^2}{1+(f/f_{0ij})^2} \right)^2} \right]^{0.5}. \quad (10)$$

It is worth mentioning that while the subfaults are not identical, M_{0ij} would be expressed based on its slip weight as described by Eq. (11):

$$M_{0ij} = \frac{M_0 S_{ij}}{\sum_{l=1}^{nl} \sum_{k=1}^{nw} S_{kl}}, \quad (11)$$

where nl and nw are the number of subfaults along the length and width of the main fault, respectively ($N = nl \times nw$); and S_{ij} is the relative slip weight of the ijth subfault [25]. In this model, the frequency content of the simulated ground motion of each subfault is controlled by the rupture history, and the corner frequency is decreasing with time, as the extent of the rupture area increases. The major advantage of the dynamic corner frequency model is that the energy content of high frequency seismic waves is conserved. Also, the simulation does not depend on the size of the subfault, and the duration of slip pulses is shorter than the duration of the fault rupture.

4.4. Determination of quality factor $Q(f)$ by nonlinear regression analysis

Various methods have been proposed for estimating the anelastic attenuation characteristics of seismic waves travelling in the rock crust. This is typically quantified by a function, $Q(f)$, through the analysis of P waves, S waves, coda waves or

Table 3: Coefficients for estimating Fourier amplitude spectrum obtained by nonlinear regression analysis of the ground motion data recorded in Tabas earthquake.

Frequency (Hz)	c_1	c_2
0.2	−0.315	−0.00488
0.6	−0.201	−0.00403
0.8	−0.0198	−0.00717
1	0.0137	−0.007
2	0.0374	−0.00682
3	−0.0897	−0.00614
4	−0.0954	−0.00560
5	−0.0608	−0.00546
6	−0.0973	−0.00605
7	−0.230	−0.00615
8	−0.287	−0.00668
9	−0.349	−0.00670
10	−0.371	−0.00760
12	−0.548	−0.00756

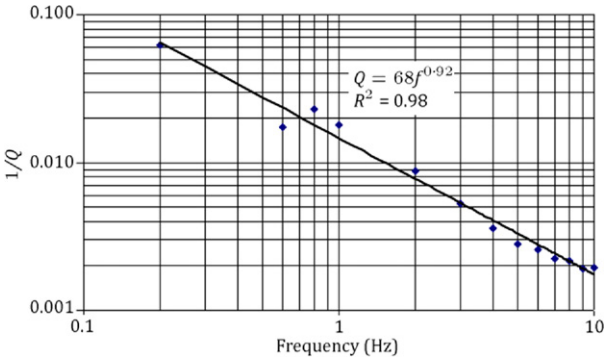

Figure 6: Regional frequency-dependent Q-value determined by nonlinear regression analysis.

Lg waves [50]. In this study, the mean frequency-dependent quality factor, $Q(f)$, was estimated using a nonlinear regression analysis of the recorded Fourier amplitude spectra. This analysis was conducted using data recorded at nine stations (as summarized in Table 2). Uncorrected strong motion data were processed to make baseline and instrumental corrections. High-pass filtering was carried out using the Butterworth filter.

The following expression was adopted for modelling the Fourier amplitude at each frequency:

$$\log a_j = c_1 + b \log R_j + c_2 R_j, \quad (12)$$

where a_j is the spectral amplitude of earthquake ground motion recorded at station j; R_j is the hypocentral distance (km); and b is the geometric spreading coefficient (as adopted in [25]), which can be expressed as follows:

$$b = \begin{cases} -1 & R_j \le 70 \\ 0 & 70 < R_j \le 130 \\ -0.5 & 130 < R_j \end{cases} \quad (13)$$

c_1 and c_2 are empirically determined coefficients that have been obtained by nonlinear regression analysis and are summarized in Table 3. According to [51], the coefficient, c_2, that represents anelastic attenuation, is inversely proportional to the quality factor, Q, expressed as $Q = -(\pi f)/(\ln(10) c_2 \beta)$. Based on the estimated values of c_2, the associated mean frequency-dependent quality factor of $Q = 68f^{0.92}$ was obtained (as shown in Figure 6). This Q value is supported by the pioneer study of seismic wave attenuation in the region conducted by Ma'hood and Hamzehloo [52], which gives the result

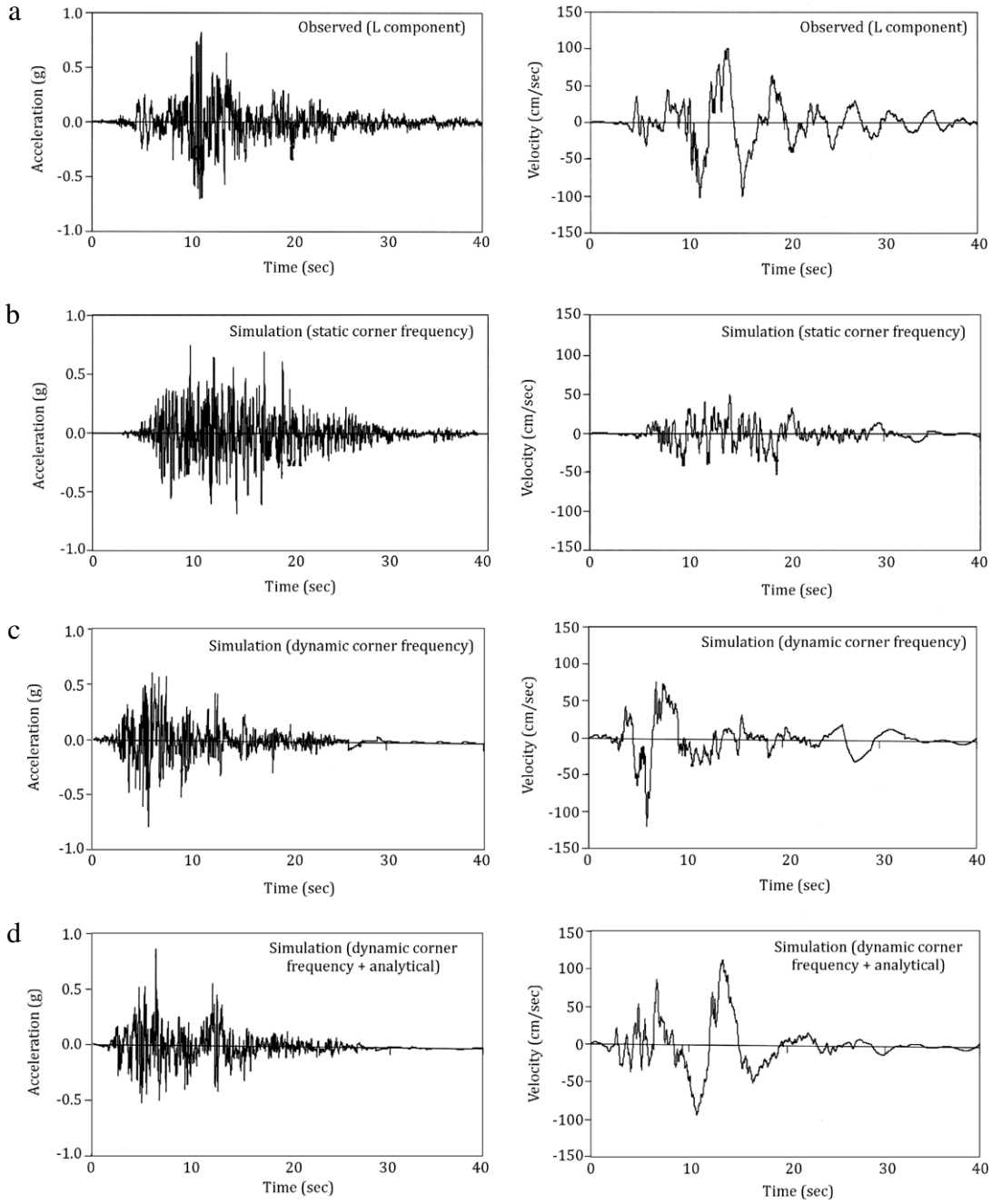

Figure 7: (a) Recorded acceleration and velocity time series and the corresponding simulation results based on (b) static corner frequency, (c) dynamic corner frequency, and (d) combination of dynamic corner frequency with the analytical model of long-period pulse.

as $Q = (101 \pm 6)f^{(0.94\pm0.11)}$. It was estimated for the regions of Zarand, Jiroft and Bam, in east central Iran, using a single back-scattering model of S-coda envelopes.

4.5. Other modelling parameters

The area of the whole fault plane was estimated as 85 km (length) × 25 km (width), based on the empirical relationship developed by Wells and Coppersmith [53], which is consistent with that reported in [3] (length = 85 km; width = 23 km) and Walker et al. [4] (length = 90 km). The distribution of the hypocenter is in accordance with the strike and dip angle of the focal mechanism, (strike, dip, slip) = (332, 31, 110), of the mainshock [3]. The hypocenter was located at a depth of 9 km, which was estimated using body wave inversion, as reported in [4]. The material properties in the vicinity of the seismic source, represented by density, ρ, and shear wave velocity, β, were determined to be 2.7 g/cm^3 and 3.5 km/s, respectively, based on the Global Crustal Model CRUST2.0 [54]. This model has been successfully used by various researchers for estimation of attenuation properties in earthquake ground-motion simulation for various seismo-tectonic conditions in the world [55,56].

Stress drop and pulsing area percentage are two key model parameters that control the amplitude of spectra at high and low frequencies, respectively. These two parameters could

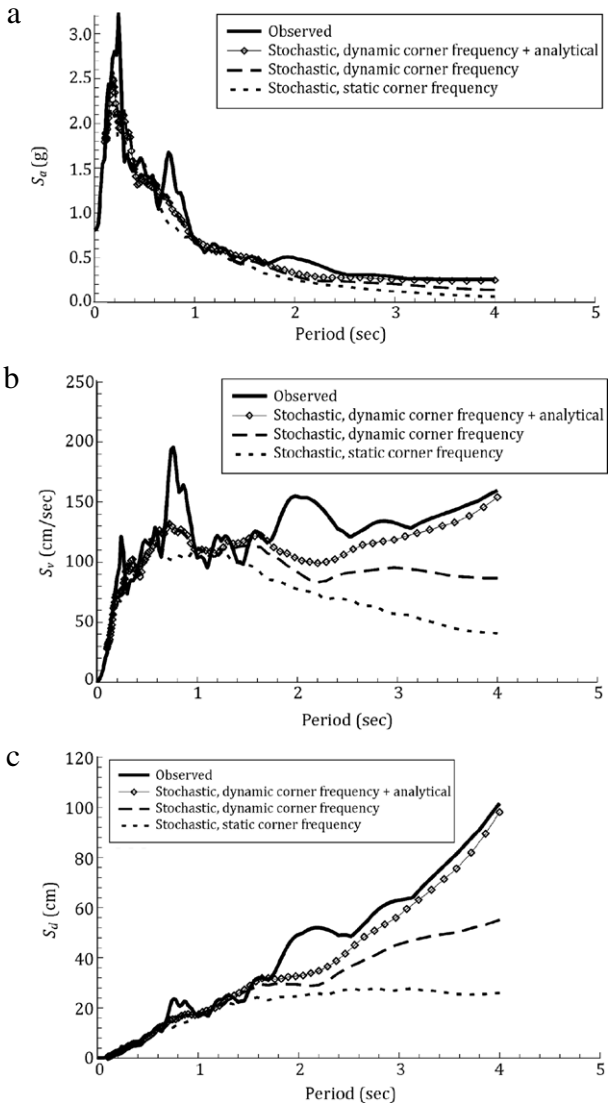

Figure 8: Recorded and simulated (a) pseudo-acceleration, (b) pseudo-velocity, and (c) displacement response spectra (5% damped) based on static corner frequency, dynamic corner frequency and combination of dynamic corner frequency with the analytical model of long-period pulse.

be calibrated using recorded near-source ground motion, as anelastic attenuation and post-critical reflection from Moho are negligible in near-source motion. The calibrated values of these two parameters are 120 bar and 25%, respectively. The stress drop parameter adopted in this study is consistent with the main sub-event of the 1978 Tabas earthquake that showed a stress drop of 100 bar [57].

A pulsing area of 25% means that at most 25% of all subfaults are contributing to the dynamic corner frequency at any time during the rupture. This value is consistent with that adopted in [25,26] for simulation of the M6.7, 1994 Northridge and M6.5, 2003 Bam earthquakes, respectively.

The effects of near-surface attenuation were taken into account by suppressing the simulated spectra using factor $\exp(-\pi f \kappa)$, as in Eq. (8). The decay parameter kappa (κ) of the region was determined by averaging over the estimates from recorded acceleration amplitude spectra and the value was found to be 0.06 [1], which is consistent with the value adopted in [26] for the M 6.5 Bam, Iran earthquake of 26 December 2003. Such a value is justified from a number of relevant studies in the USA and Europe (as reported in [55]). Crustal site amplification was estimated using the *square-root-impedance method* proposed by Boore and Joyner [58] for rock sites, characterized by the average shear wave velocity over the upper 30 m ($\bar{V}_{30}$) of 620 m/s.

For the analytical model of Mavroeidis and Papageorgiou [23], there are four main input parameters, namely; pulse amplitude (Amp), prevailing frequency (f_p), phase angle (ν) and oscillatory characteristic (γ). Calibrations have been conducted and the corresponding values for Amp, ν and γ, are 105°, 180° and 2.2°, respectively. The parameter, f_p, is the reciprocal of the pulse duration (T_p) that was calculated using Eq. (4) [23], as reported in the first part of this paper.

The full set of recommended modelling parameters has been summarized and tabulated in Table 4.

4.6. Simulation results

Ground motion of the 1978 Tabas (Iran) earthquake recorded at the Tabas station has been simulated using finite-fault stochastic modelling, based on the dynamic corner frequency [25] and incorporated with the analytical model for mimicking near-source pulse characteristics [23]. Figure 7 shows the recorded and simulated acceleration and velocity time series at the Tabas station. Simulation results using static corner frequency and dynamic corner frequency, without incorporating the analytical model for pulse characteristics, have also been included in Figure 7 for direct comparison. It is evidenced that the results using finite-fault stochastic modelling, based on dynamic corner frequency and analytical modelling (Figure 7(d)), demonstrate the best match with actual recordings. In particular, the pulse period and the amplitude are shown to be very close in the velocity time series.

The corresponding 5% damped response spectra are also compared. The three sets of simulated results have been plotted in Figure 8 and superimposed with the recorded spectra. In Figure 8(a), pseudo-acceleration response spectra have been plotted. It is shown that the simulation results are broadly consistent with actual recordings, with a relatively larger discrepancy at a short-period range. No significant difference can be observed between the spectra simulated using different models. Pseudo-velocity and displacement response spectra have been plotted in Figure 8(b) and (c), from which substantial differences can be seen between the three simulated results. Large discrepancies can be observed for periods greater than 1.5 s, and the differences become larger for longer periods. It is important to note that the spectra simulated using finite-fault stochastic modelling, based on dynamic corner frequency and the analytical near-source pulse model, provide the best match with the recorded spectra. The modelling based on static corner frequency is not capable of modelling the large pulse of near-source ground motion and substantial differences from the observed response spectra can be seen, particularly in long period ranges (i.e. $T > 1.5$ s). Figure 9 demonstrates the consistency of the Fourier spectral amplitudes of the parallel and normal component of motions recorded at the Tabas station. The predicted time series, based on the seismological model developed in this study, with incorporation of dynamic corner frequency and the analytical near-source pulse model at the Deyhook station (with a hypocentral distance of 18 km, refer to Table 2) and the corresponding acceleration response spectra (S_a) are also consistent with the observed motion (the mean of two horizontal components), as shown in Figures 10 and 11.

Table 4: Summary of the parameters for modelling near-fault ground motion recorded at Tabas station.

Parameters/items	Values and references
Fault model	Finite-fault model Dimension of fault plane = 85 km (length) [53] 25 km (width) Dimension of each sub-fault = 5 km (length/width) Stress drop = 120 bar Pulsing area percentage = 25% Slip distribution = random
Crustal properties at the vicinity of seismic source	Shear wave velocity $\beta = 3.5$ km/s Density $\rho = 2.7$ g/cm^3 [54]
Near-fault pulse characteristic	Pulse amplitude (A_{mp}) = 105 Prevailing frequency (f_p) = 0.174 s^{-1} Phase angle (ν) = 180° Oscillatory characteristic (γ) = 2.2 (calibrated in this study)
Geometric spreading	$1/R$ [45]
Anelastic attenuation	$Q = 68f^{0.92}$ (obtained in this study)
Upper crustal amplification	Square-root-impedance method with crustal profiles of generic rock site [58]
Near-surface attenuation	$\kappa = 0.06$ [1]
Window function	Saragoni-Hart model

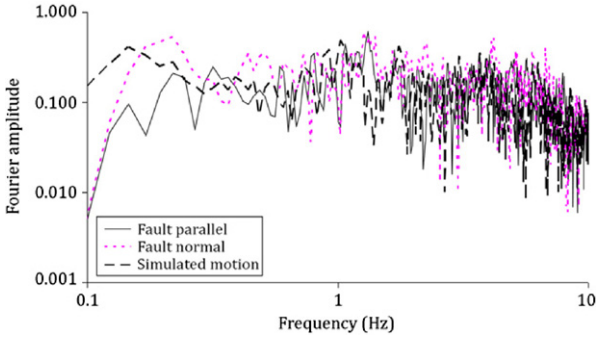

Figure 9: Fourier spectral amplitudes of simulated motions along with the parallel and normal components of the motions recorded at Tabas station.

5. Conclusions

In the first part of this study, the near-source characteristics of strong ground motion recorded in the M7.4 1978 Tabas, Iran, earthquake have been examined. The horizontal acceleration time series recorded by the Tabas station (TAB), located in the forward-directivity region, have been filtered and rotated into directions perpendicular and parallel to the fault rupture. The fault-normal component of the ground motion shows an obvious peak in the long-period range (greater than 4 s) of the velocity response spectrum. The duration of the velocity pulse recorded at the Tabas station could be well predicted by the equations of Mavroeidis and Papageorgiou [23] and Baker [31]. On the other hand, the value of the peak ground velocity predicted by the equation proposed by Bray and Rodriguez-Marek [15] is around 20% different from the recorded value. The ratio of fault-parallel to fault-normal peak ground velocity observed in the records is within one standard deviation from that predicted by Bray and Rodriguez-Marek [15]. Also, the good match with the ratio of the fault-normal horizontal response spectrum to the average horizontal response spectrum proposed by Somerville et al. [14] provides strong evidence of the existence of forward directivity effects in the ground motion recorded at the Tabas station.

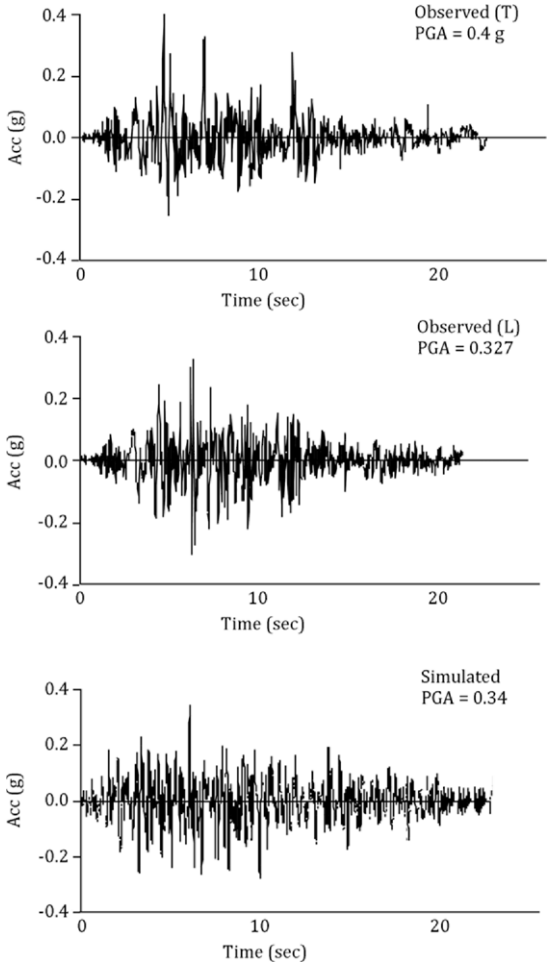

Figure 10: The parallel and normal components of acceleration time histories recorded at Deyhook station and the corresponding simulation results.

In the second part of the study, stochastic simulation using an extended finite-fault model based on the new definition of the corner frequency, namely, "dynamic corner

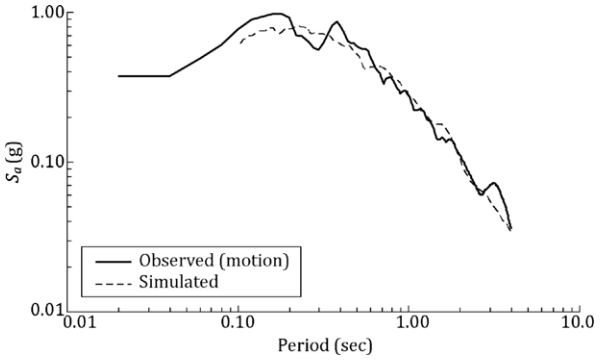

Figure 11: Observed motion (mean of two horizontal components) and simulated acceleration response spectra (S_a) at Deyhook station.

frequency'', has been combined with the analytical method of Mavroeidis and Papageorgiou [23] for modelling the impulsive long-period ground motion recorded at the Tabas station and a new set of modelling parameters has been recommended. The simulation results have been compared with the case computed using static corner frequency, and that using dynamic corner frequency, without incorporating the analytical pulse model. Figures 7 and 8 show clearly that the use of the stochastic method based on dynamic corner frequency and incorporated with the analytical model could accurately model near-field ground motion at both low and high frequency ranges, as well as the impulsive characteristics of the motion. As a distinct velocity pulse can be clearly observed in this recorded time series, ordinary stochastic simulations of the seismological model are not capable of mimicking near-fault pulse characteristics. Significant discrepancies can be observed predominantly at long period ranges (greater than 1.5 s) between various simulation results.

Acknowledgments

The generosity of Dariush Motazedian and Gail Atkinson for providing us with the source code of the EXSIM program is gratefully acknowledged.

References

[1] Shoja-Taheri, J. and Anderson, J. "The 1978 Tabas, Iran, earthquake: an interpretation of the strong motion records", *Bull. Seismol. Soc. Amer.*, 78(1), pp. 142–171 (1988).
[2] Mohajer-Ashjai, A. and Nowroozi, A.A. "The Tabasc earthquake of September 16, 1978 in east central Iran: a preliminary field report", *Geophys. Res. Lett.*, 6, pp. 689–692 (1979).
[3] Berberian, M. "Earthquake faulting and bedding thrust associated with the Tabas-e-Golshan (Iran) earthquake of September 16, 1978", *Bull. Seismol. Soc. Amer.*, 69, pp. 1861–1887 (1979).
[4] Walker, J., Jackson, J. and Baker, C. "Surface expression of thrust faulting in eastern Iran: source parameters and surface deformation of the 1978 Tabas and 1968 Ferdows earthquake sequences", *Geophys. J. Int.*, 152, pp. 749–765 (2003).
[5] Housner, G.W. and Trifunac, M.D. "Analysis of accelerograms: parkfield earthquake", *Bull. Seismol. Soc. Amer.*, 57, pp. 1193–1220 (1967).
[6] Boore, D. and Zoback, M. "Two dimensional kinematic fault modelling of the Pacoima Dam strong motion records of February 9, 1991, San Fernando earthquake", *Bull. Seismol. Soc. Amer.*, 64, pp. 555–570 (1974).
[7] Pitarka, A., Irikura, K., Iwata, T. and Sekiguchi, H. "Three-dimensional simulation of the near-fault ground motion for the 1995 Hyogo-ken Nanbu (Kobe), Japan, earthquake", *Bull. Seismol. Soc. Amer.*, 88, pp. 428–440 (1998).
[8] Stephenson, W.J., Williams, R.A., Odum, J.K. and Worley, D.M. "High-resolution seismic reflection surveys and modelling across an area of high damage from the 1994 Northridge earthquake, Sherman Oaks, California", *Bull. Seismol. Soc. Amer.*, 90, pp. 643–654 (2000).
[9] Alavi, B. and Krawinkler, H. "Effects of near-field ground motion on frame structures", John A. Blume Earthquake Engineering Center, Report No.138, Department of Civil and Environmental Engineering, Stanford University, Stanford, CA, p. 301 (2001).
[10] Chi, W., Dreger, D. and Kaverina, A. "Finite-source modelling of the 1999 Taiwan (Chi-Chi) earthquake derived from a dense strong-motion network", *Bull. Seismol. Soc. Amer.*, 91(5), pp. 1115–1144 (2001).
[11] Shoja-Taheri, J. and Ghofrani, H. "Stochastic finite-fault modelling of strong ground motions from the 26 December 2003 Bam, Iran, earthquake", *Bull. Seismol. Soc. Amer.*, 97(6), pp. 1950–1959 (2007).
[12] Baker, J.W. and Cornell, C.A. "Vector-valued ground motion intensity measures for probabilistic seismic demand analysis", John A. Blume Earthquake Engineering Center, Report No. 150, Stanford University, Stanford, CA, p. 321 (2005).
[13] Fu, Q. "Modeling and prediction of fault-normal near-field ground motions and structural response", Ph.D. Dissertation, Department of Civil and Environmental Engineering, Stanford University, Stanford, CA, p. 231 (2005).
[14] Somerville, P.G., Smith, N.F., Graves, R.W. and Abrahamson, N.A. "Modification of empirical strong ground motion attenuation relations to include the amplitude and duration effects of rupture directivity", *Seismol. Res. Lett.*, 68, pp. 199–222 (1997).
[15] Bray, J.D. and Rodriguez-Marek, A. "Characterization of forward-directivity ground motions in the near-fault region", *Soil Dyn. Earthq. Eng.*, 24, pp. 815–828 (2004).
[16] Bertero, V.V., Mahin, S.A. and Herrera, R.A. "A seismic design implications of near-fault San Fernando earthquake records", *Earthq. Eng. Struct. Dyn.*, 6, pp. 31–42 (1978).
[17] Naeim, F. "On seismic design implications of the 1994 Northridge earthquake record", *Earthq. Spectra*, 11(1), pp. 91–109 (1995).
[18] Makris, N. "Rigidity-plasticity-viscosity: can electro rheological dampers protect base-isolated structures from near-source ground motions", *Earthq. Eng. Struct. Dyn.*, 26, pp. 571–591 (1997).
[19] Chopra, A.K. and Chintanapakdee, C. "Comparing response of SDOF systems to near-fault and far-fault earthquake motions in the context of spectral regions", *Earthq. Eng. Struct. Dyn.*, 30, pp. 1769–1789 (2001).
[20] Anderson, J.C. and Bertero, V. "Uncertainties in establishing design earthquakes", *J. Struct. Eng.*, 113, pp. 1709–1724 (1986).
[21] Hall, J.F., Heaton, T.H., Halling, M.W. and Wald, D.J. "Near-source ground motions and its effects on flexible buildings", *Earthq. Spectra*, 11, pp. 569–605 (1995).
[22] Iwan, W.D. "Drift spectrum: measure of demand for earthquake ground motions", *J. Struct. Eng.*, 123(4), pp. 397–404 (1977).
[23] Mavroeidis, G.P. and Papageorgiou, A.S. "A mathematical representation of near-fault ground motions", *Bull. Seismol. Soc. Amer.*, 3, pp. 1099–1131 (2003).
[24] Gabor, D., *Theory of Communication. I. The Analysis of Information*, vol. 93, IEEE pp. 429–441 (1946).
[25] Motazedian, D. and Atkinson, G. "Stochastic finite-fault modelling based on a dynamic corner frequency", *Bull. Seismol. Soc. Amer.*, 95(2), pp. 995–1010 (2005).
[26] Motazedian, D. and Moinfar, A. "Hybrid stochastic finite fault modelling of 2003, M6.5, Bam earthquake (Iran)", *J. Seismolog.*, 10, pp. 91–103 (2006).
[27] Yaghmaei-Sabegh, S. "Detection of pulse-like ground motions based on continues wavelet transform", *J. Seismolog.*, 14, pp. 715–726 (2010).
[28] Engdahl, E.R., van der Hilst, R. and Buland, R. "Global teleseismic earthquake relocation with improved travel times and procedures for depth determination", *Bull. Seismol. Soc. Amer.*, 88, pp. 722–743 (1998).
[29] Somerville, P.G. "Magnitude scaling of the near fault rupture directivity pulse", *Phys. Earth Planet. Inter.*, 137(1), pp. 1–12 (2003).
[30] Akkar, S., Yazgan, U. and Gulkan, P. "Drift estimates in frame buildings subjected to near-fault ground motions", *J. Struct. Eng.*, 131(7), pp. 1014–1024 (2005).
[31] Baker, J.W. "Quantitative classification of near-fault ground motions using wavelet analysis", *Bull. Seismol. Soc. Amer.*, 97, pp. 1486–1501 (2007).
[32] Hollingsworth, J., Jackson, J. and Alarcon, J.E. "The 4th February 1997 Bojnurd (Garmkhan) earthquake in NE Iran: field, teleseismic, and strong-motion evidence for rupture directivity effects on a strike-slip fault", *J. Earthq. Eng.*, 11, pp. 193–214 (2007).
[33] Hanks, T. and McGuire, R. "The character of high-frequency strong ground motion", *Bull. Seismol. Soc. Amer.*, 71, pp. 2071–2095 (1981).
[34] Atkinson, G. and Boore, D. "New ground motion relations for eastern North America", *Bull. Seismol. Soc. Amer.*, 85, pp. 17–30 (1995).
[35] Atkinson, G.M. and Boore, D.M. "Stochastic point-source modelling of ground motions in the Cascadia region", *Seismol. Res. Lett.*, 68, pp. 74–85 (1997).
[36] Toro, G., Abrahamson, N. and Schneider, J. "Model of strong ground motion in eastern and central North America: best estimates and uncertainties", *Seismol. Res. Lett.*, 68, pp. 41–57 (1997).
[37] Lam, N., Wilson, J. and Hutchinson, G. "Generation of synthetic earthquake accelerograms using seismological modelling: a review", *J. Earthq. Eng.*, 4(3), pp. 321–354 (2000).
[38] Atkinson, G. and Silva, W. "Stochastic modelling of California ground motions", *Bull. Seismol. Soc. Amer.*, 90, pp. 255–274 (2000).
[39] Nicknam, A., Yazdani, A. and Yaghmaei-Sabegh, S. "Predicting probabilistic-based strong ground motion time series for Citadel of Arg-e-Bam (South-East Iran)", *J. Earthq. Eng.*, 13, pp. 482–499 (2009).

[40] Boore, D. "Prediction of ground motion using the stochastic method", *Pure Appl. Geophys.*, 160, pp. 635–676 (2003).
[41] Brune, J.N. "Tectonic stress and the spectra of seismic shear waves from earthquakes", *J. Geophys. Res.*, 75, pp. 4997–5009 (1970).
[42] Brune, J. "Correction", *J. Geophys. Res.*, 76, p. 5002 (1971).
[43] Boore, D. "Stochastic simulation of high-frequency ground motions based on seismological models of the radiated spectra", *Bull. Seismol. Soc. Amer.*, 73, pp. 1865–1894 (1983).
[44] Anderson, J. and Hough, S. "A model for the shape of the Fourier amplitude spectrum of acceleration at high frequencies", *Bull. Seismol. Soc. Amer.*, 74, pp. 1969–1993 (1984).
[45] Beresnev, I.A. and Atkinson, G. "Stochastic finite-fault modelling of ground motions from the 1994 Northridge, California earthquake. I. Validation on rock sites", *Bull. Seismol. Soc. Amer.*, 88, pp. 1392–1401 (1998).
[46] Hartzell, S. "Earthquake atershocks as Green's functions", *Geophys. Res. Lett.*, 5, pp. 1–4 (1978).
[47] Somerville, P., Sen, M. and Cohee, B. "Simulations of strong ground motions recorded during the 1985 Michoacan, Mexico and Valparaiso, Chile earthquakes", *Bull. Seismol. Soc. Amer.*, 81, pp. 1–27 (1991).
[48] Tumarkin, A. and Archuleta, R. "Empirical ground motion prediction", *Ann. Geofis.*, 37, pp. 1691–1720 (1994).
[49] Zeng, Y., Anderson, J. and Yu, G. "A composite source model for computing realistic synthetic strong ground motions", *Geophys. Res. Lett.*, 21(8), pp. 725–728 (1994).
[50] Ma'hood, M., Hamzehloo, H. and Doloei, G.J. "Attenuation of high frequency P and S waves in the crust of the East-Central Iran", *Geophys. J. Int.*, 179, pp. 1669–1678 (2009).
[51] Atkinson, G. and Mereu, R. "The shape of ground motion attenuation curves in south-eastern Canada", *Bull. Seismol. Soc. Amer.*, 82, pp. 2014–2031 (1992).
[52] Ma'hood, M. and Hamzehloo, H. "Estimation of coda wave attenuation in east central Iran", *J. Seismolog.*, 13(1), pp. 125–139 (2009).
[53] Wells, D. and Coppersmith, K. "New empirical relationships among magnitude, rupture length, rupture width, rupture area, and surface displacement", *Bull. Seismol. Soc. Amer.*, 84, pp. 974–1002 (1994).
[54] Global Crustal Model CRUST2.0, Institute of geophysics and planetary physics, University of California, San Diego (2001). http://mahi.ucsd.edu/Gabi/rem.dir/crust/crust2.html.
[55] Chandler, N.T.K. Lam and Tsang, H.H. "Near-surface attenuation modelling based on rock shear-wave velocity profile", *Soil Dyn. Earthq. Eng.*, 26, pp. 1004–1014 (2006).
[56] Lam, N.T.K., Wilson, J.L., Chandler, A.M. and Hutchinson, G.L. "Response spectrum predictions for potential near-field and far-field earthquakes affecting Hong Kong: rock sites", *Soil Dyn. Earthq. Eng.*, 22, pp. 47–72 (2002).
[57] Sarkar, I., Sriram, V., Hamzehloo, H. and Khattri, K.N. "Sub event analysis for the Tabas earthquake of September 16, 1978, using near field accelerograms", *Phys. Earth Planet. Inter.*, 151, pp. 53–76 (2005).
[58] Boore, D.M. and Joyner, W.B. "Site amplification for generic rock sites", *Bull. Seism. Soc. Am.*, 87, pp. 327–341 (1997).

Saman Yaghmaei-Sabegh obtained his Ph.D. degree from Iran University of Science and Technology and was awarded the Elite Prize by the university in 2006 and 2007. He is currently Assistant Professor at Tabriz University and has been Visiting Scholar at The University of Melbourne, Australia since 2007. He is Member of the Iranian Earthquake Engineering Association. He has published some 30 technical articles and won an award at the 14th International Conference on Earthquake Engineering in 2008, as a young researcher.

Hing-Ho Tsang obtained his Ph.D. degree from The University of Hong Kong and was awarded the Li Ka Shing Prize and Norman W.M. Ko Ph.D. Prize for the best thesis of the year by the university. He is currently Research Fellow at The University of Hong Kong and has been Visiting Scholar at The University of Melbourne, Australia since 2004. He is Member of the American Society of Civil Engineers and Director of its Hong Kong Section.

Hing-Ho is regularly invited to give lectures internationally, notably including a keynote speech delivered at the Australian Earthquake Engineering Conference in 2008. He has published some 70 technical articles and has won the Endeavour Australia Cheung Kong Award from the Australian Government, the Hsai-Yang Fang Research Award from The International Society of Environmental Geotechnology and the Highly Commendable Paper Award at the Sixth International Conference on Shock and Impact Loads on Structures.